Available online at www.sciencedirect.com

ScienceDirect

Trans. Nonferrous Met. Soc. China 27(2017) 868−875

Transactions of Nonferrous Metals Society of China

www.tnmsc.cn

Hydrothermal synthesis and enhanced photocatalytic activity of hierarchical flower-like Fe-doped $BiVO_4$

Hai-bin LI, Jian ZHANG, Guo-you HUANG, Sheng-hao FU, Chao MA,
Bai-yu WANG, Qian-ru HUANG, Hong-wei LIAO

School of Materials Science and Engineering,
Changsha University of Science and Technology, Changsha 410114, China

Received 11 April 2016; accepted 15 December 2016

Abstract: Fe-doped $BiVO_4$ with hierarchical flower-like structure was prepared via a hydrothermal method using sodium dodecyl benzene sulfonate (SDBS) as structure directing agent. X-ray diffraction (XRD), scanning electron microscope (SEM), transmission electron microscope (TEM), high resolution transmission electron microscope (HRTEM), X-ray photoelectron spectroscopy (XPS) and UV-Vis were applied for characterization of the as-prepared samples. The formation mechanism of flower-like structure was proposed based on the evolution of morphology as a function of hydrothermal time. Fe-doped into substitutional sites of $BiVO_4$ effectively improved the migration and separation of photogenerated carrier and enhanced the utilization of visible light. Flower-like Fe-doped $BiVO_4$ showed much higher visible-light-driven photocatalytic efficiency for degradation of methyl blue compared with the pristine $BiVO_4$. And the sample with a Fe/Bi mole ratio of 2.5% showed the highest photocatalytic efficiency.

Key words: $BiVO_4$; hydrothermal method; Fe doping; photocatalysis

1 Introduction

In past decades, semiconductor photocatalysis has received a great deal of attention due to its potential for environmental pollution treatment [1]. Titanium dioxide (TiO_2) is considered as one of the most promising photocatalysts due to its high activity, low cost, nontoxicity, and chemical stability in aqueous solution. However, TiO_2 can only utilize the UV lights due to its wide band gap (3.2 eV), which limits its industrial application [2]. In order to effectively make use of the sunlight, it is important to find the semiconductors with high visible light photocatalytic activities.

In recent years, some Bi-based oxides, such as Bi_2O_3 [3], Bi_2WO_6 [4], $Bi_2O_2CO_3$ [5], and $BiVO_4$ [6,7] have gained wide attention because of their visible-light-driven photocatalytic abilities. $BiVO_4$ is a binary complex oxide, which mainly exists in three crystalline phases: monoclinic scheelite structure, tetragonal zircon structure, and tetragonal scheelite structure [8]. Monoclinic $BiVO_4$ (m-$BiVO_4$) is widely accepted as a promising visible-light-driven photocatalyst due to its narrow band gap of 2.4 eV [6−8]. However, the high electron-hole recombination decreases its quantum yield and photocatalytic activity [9]. Moreover, the light response range of $BiVO_4$ still needs to be further broadened. The previous work revealed that larger distortions of BiO_6 octahedron and VO_4^{3-} tetrahedron in m-$BiVO_4$ led to a larger inner potential and more overlap of Bi 6s and O 2p orbitals in the valence band [8], respectively, which could accelerate the migration of carriers and facilitate the separation of photogenerated electrons and holes, leading to higher quantum yield. Doping with impurity metal ions has been proved to be an effective strategy to enlarge the distortions of BiO_6 octahedrons and VO_4^{3-} tetrahedrons, as a part of Bi^{3+} or V^{5+} ions in m-$BiVO_4$ are substituted by impurity ions with different ionic radius [10]. It is also an effective way to expand the light absorption range of m-$BiVO_4$ by creating impurity levels in the forbidden band [11]. Fe^{3+} has been widely used for semiconductor oxide doping due to its half-filled electronic configuration [12]. However, to the best of our knowledge, there are few reports on the synthesis and properties of Fe-doped $BiVO_4$ [13].

Foundation item: Project (51102025) supported by the National Natural Science Foundation of China; Project (14JJ7040) supported by Natural Science Foundation of Hunan Province, China; Project (2014GH561172) supported by China Torch Program

Corresponding author: Hai-bin LI; Tel: +86-731-85258232; Fax: +86-731-82309128; E-mail: coastllee@hotmail.com

DOI: 10.1016/S1003-6326(17)60102-X

It was reported that the activities of photocatalysts are not only related to their crystal structures and phase compositions, but also affected by their morphologies [14−19]. Photocatalysts with special morphologies, such as hierarchical flower-like structures assembled by two-dimensional (2D) nanosheets, possess larger specific surface areas and open porous structures, which can effectively improve the light absorption and facilitate the contact of catalysts and substrates [20]. However, by far, no reports have been made on Fe-doped $BiVO_4$ with hierarchical flower-like structures.

Hydrothermal method has been widely used in the synthesis of photocatalytic materials because of its facility to synthesize inorganic materials with perfect crystal structures and regular shapes in an environmentally friendly way [21−24]. In the present work, Fe-doped $BiVO_4$ with hierarchical flower-like structures was prepared via a sodium dodecyl benzene sulfonate (SDBS) assisted hydrothermal method. The photocatalytic properties of the as-prepared samples were assessed by photodegradation of methyl blue (MB).

2 Experimental

2.1 Synthesis of Fe-doped $BiVO_4$

All reagents were of analytical reagent grades and used without further purification. Distilled water was used in all experiments. In a typical synthesis, 0.001 mol of $Bi(NO_3)_3\cdot 5H_2O$ and a certain amount of $Fe(NO_3)_3\cdot 9H_2O$ (Fe/Bi mole ratios were controlled at 0, 1%, 2.5%, 5%, and 7.5%) were dissolved in 25 mL of glacial acetic acid, while 0.001 mol of $Na_3VO_4\cdot 12H_2O$ was dissolved in 55 mL of distilled water under constant stirring. The obtained solutions were then mixed together, followed by the adding of 5 g of $CO(NH_2)_2$ and 0.5 g of SDBS. After being stirred for 30 min, the suspension was transferred into a 100 mL Teflon-lined autoclave stainless steel autoclave. The autoclave was heated at 160 °C for 15 h, and then cooled to room temperature naturally. The product was collected, washed with distilled water and absolute alcohol three times, respectively, and finally dried at 80 °C for 20 h to obtain Fe-doped $BiVO_4$.

2.2 Characterization

X-ray diffraction (XRD) analysis was conducted on a Rigaku D/Max 2500 powder diffractometer with Cu K_α radiation (λ=1.5406 Å). Scanning electron microscopy (SEM) imaging was performed on a FEI SIRION 200 field emission scanning electron microscope. Transmission electron microscopy (TEM) and high resolution transmission electron microscopy study (HRTEM) were carried out on a Philips Tecnai 20 G2 S-TWIN electron microscope. X-ray photoelectron spectroscopy (XPS) analysis was proceeded on a K-Alpha 1063 electron spectrometer from Thermo Fisher Scientific using 72W Al K_α radiation. Raman spectra of the samples were obtained with RFS100/S FT-Raman apparatus from Bruker. UV-Vis diffuse reflectance spectra (UV-vis) were measured with a Specord 200 UV spectrophotometry. The BET surface areas of the samples were analyzed by a Micromeritics ASAP2020 equipment.

2.3 Photocatalytic experiments

The photocatalytic activities of the samples were evaluated by photodegradation of MB under visible light irradiation. A 125 W Xe lamp with a 410 nm cut-off filter was used as the light source. 0.1 g of photocatalyst was suspended in 100 mL of MB aqueous solution (20 mg/L). The mixture was magnetic stirred in the dark for 30 min before irradiation to allow the system to reach an adsorption/desorption equilibrium. The photocatalytic system was magnetically stirred during the course of illumination. At given time intervals, 5 mL suspensions were sampled and centrifuged to remove the photocatalyst powders. The concentration of MB solution was evaluated by an UNICO UV−2100 spectrophotometer at 660 nm.

3 Results and discussion

Figure 1(a) shows the XRD patterns of the as-prepared Fe-doped $BiVO_4$ with different Fe doping levels. When the Fe/Bi mole ratios were controlled at 0, 1.0%, 2.5%, and 5.0%, the characteristic diffraction peaks of each XRD pattern can be readily indexed to a pure monoclinic scheelite structure (JCPD No. 14−0688). No peaks of any other phases or impurities, such as $BiFeO_3$ or Fe_2O_3, were detected. With increasing the Fe/Bi mole ratio to 7.5%, a characteristic diffraction peak at 2θ=24.5° appears, which is assigned to tetragonal $BiVO_4$ (JCPDS No. 75−1866), suggesting that a relative high Fe/Bi mole ratio may lead to a phase transition from monoclinic to tetragonal. It was reported that monoclinic scheelite $BiVO_4$ is a thermodynamically stable phase compared with tetragonal $BiVO_4$, so hydrothermal reaction usually generates m-$BiVO_4$ [25]. However, if a relatively high concentration of impurity ions enters the crystal lattice in the process of $BiVO_4$ crystallization, it will cause the crystal lattice distortion, resulting in the phase transition from monoclinic to tetragonal. Figure 1(b) exhibits the magnified view of (121) and (040) diffraction peaks of all the samples, which show gradual shifts of peaks toward lower angles with increasing Fe doping level and the maximum shifting of 0.15° for the (121) peak is reached at 7.5% doping. The peak shift may be ascribed to the lattice expansion due to the slight portion of Fe atom incorporation, and indicates that Fe may have a certain influence on the *d* (121) and *d* (040) spacing of the monoclinic $BiVO_4$. Considering that the ionic radius of Fe^{3+} (0.064 nm) is much smaller than that of Bi^{3+} (0.103 nm) but close to that of V^{5+} (0.054 nm), the lattice expansion is much more likely to be resulted from the substitution of V^{5+} by Fe^{3+}. These XRD results indicate that Fe^{3+} has been well inserted into V^{5+} sites of the host $BiVO_4$ lattice without forming any segregated impurity phase.

The chemical states of Fe-doped $BiVO_4$ with a Fe/Bi mole ratio of 5.0% were revealed through XPS analysis. Figure 2 shows the high-resolution XPS spectra of Bi 4f, V 2p, Fe 2p, and O 1s, respectively. Two strong peaks located at 163.8 and 158.5 eV, are assigned to Bi $4f_{5/2}$ and Bi $4f_{7/2}$ (Fig. 2(a)), respectively, which confirms that the bismuth species in the $BiVO_4$ is Bi^{3+} cations [11]. Two peaks at approximately 523.6 and 516.1 eV are found in the V 2p XPS spectrum (Fig. 2(b)), which correspond to the characteristic spin-orbit splitting of V $2p_{1/2}$ and V $2p_{3/2}$ signals, respectively, indicating the presence of V^{5+} in the sample [11]. The characteristic

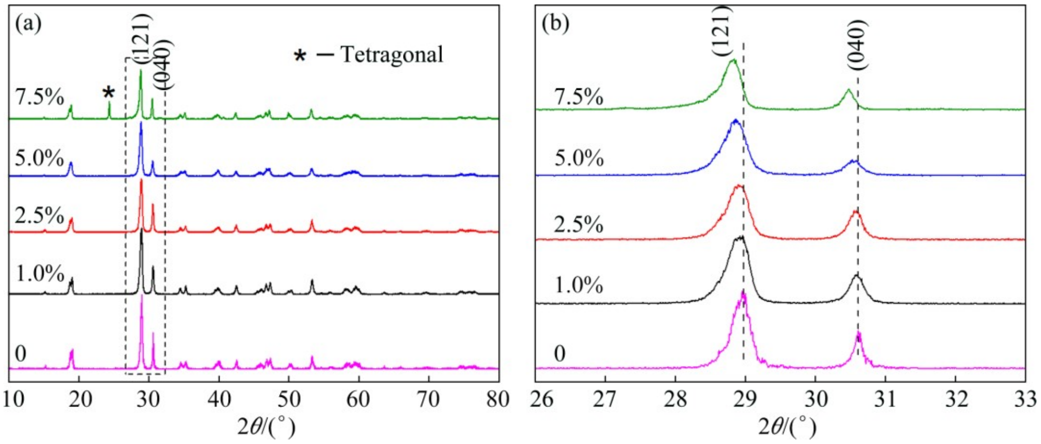

Fig. 1 XRD patterns of as-prepared samples with different Fe doping contents (a) and magnified peaks of (121) and (040) planes of as-prepared samples (b)

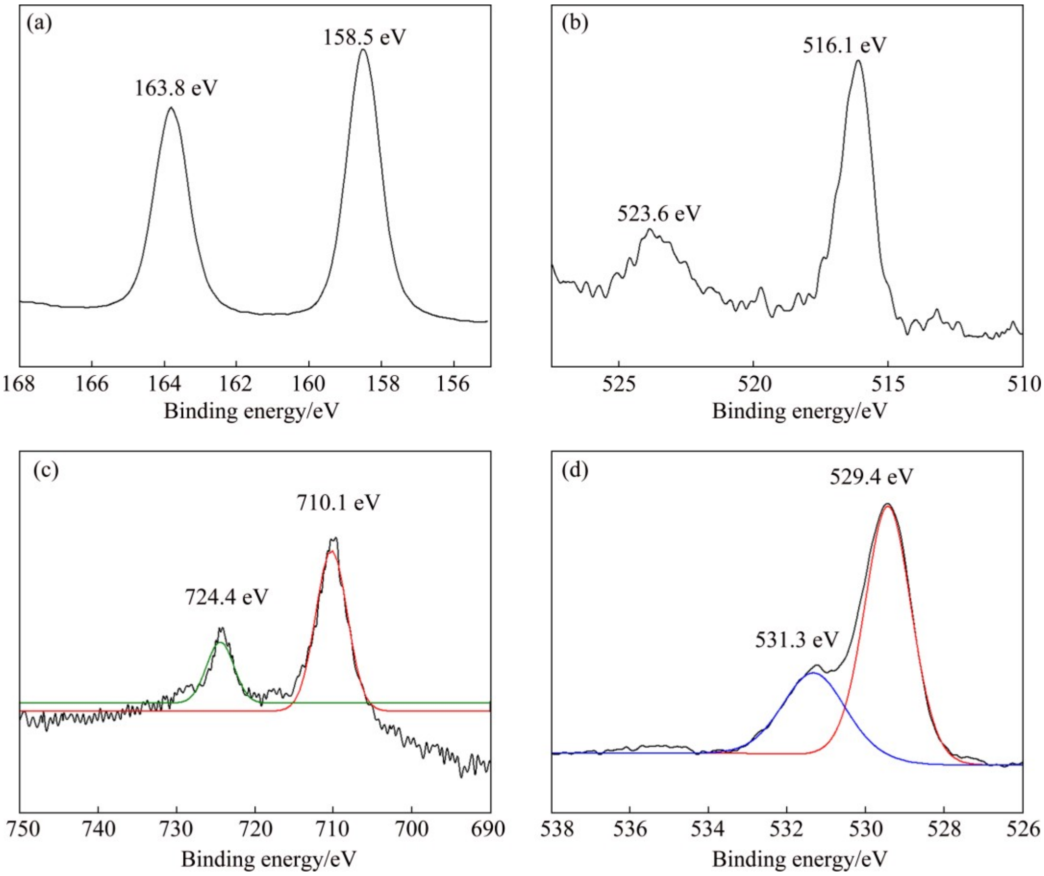

Fig. 2 High-resolution XPS spectra of Bi 4f (a), V 2p (b), Fe 2p (c), and O 1s (d) for Fe-doped $BiVO_4$ with Fe/Bi mole ratio of 5.0%

spin-orbit splitting of Fe $2p_{1/2}$ and Fe $2p_{3/2}$ signals is observed at about 724.4 and 710.1 eV (Fig. 2(c)), respectively, indicating that the iron species in the sample are Fe^{3+} cations [12]. It is interesting that the asymmetric O 1s peak of Fe-doped $BiVO_4$ can be fitted by two peaks at binding energies of 529.4 and 531.3 eV (Fig. 2(d)), which are normally assigned as the low binding energy component (LBEC) and the high binding energy component (HBEC), indicating two different kinds of O species in the sample [11]. The LBEC can be attributed to the lattice oxygen (O_{latt}), while the HBEC is resulted from the chemisorbed oxygen (O_{ads}) caused by the surface chemisorbed species such as hydroxyl and H_2O, respectively. It was reported that the HBEC component develops with the increase of oxygen vacancies in the sample [11]. Higher HBEC suggests more oxygen vacancies. The calculated ratio of O_{ads} to O_{latt} is 0.39, indicating the presence of plenty of oxygen deficiencies in the Fe-doped $BiVO_4$. The extrinsic oxygen deficiency in Fe-doped $BiVO_4$ may be ascribed to the charge compensation due to the substitution of V^{5+} by Fe^{3+} with a lower valence state. The presence of oxygen vacancies was reported to be beneficial for the enhancement in photocatalytic performance of $BiVO_4$ by promoting the separation of charge carriers.

The Raman spectra of pure $BiVO_4$ and Fe-doped $BiVO_4$ with a Fe/Bi mole ratio of 2.5% are presented in Fig. 3. Raman bands around 210, 325, 368, 819 cm^{-1} are observed for both samples, which are attributed to the external mode of $BiVO_4$, the asymmetric deformation mode of the VO_4^{3-} tetrahedron, the symmetric deformation mode of the VO_4^{3-} tetrahedron, and the stretching mode of V—O band, respectively [8,26]. It is noteworthy that the stretching mode of the shorter V—O at 819 cm^{-1} for pure $BiVO_4$ is shifted to a higher frequency of 827 cm^{-1} for Fe-doped $BiVO_4$, suggesting that Fe-doped $BiVO_4$ possesses stronger symmetry constraint and the distortion of VO_4^{3-} tetrahedron in Fe-doped $BiVO_4$ is larger than that in pure $BiVO_4$ [8]. As revealed in the previous works, the electronic structure of $BiVO_4$ was affected by distortion of the VO_4^{3-} tetrahedron in the local structure of $BiVO_4$. The larger distortion leads to more overlap of the Bi 6s and O 2p orbitals in the valence band of monoclinic $BiVO_4$, which is beneficial for the migration of photogenerated holes [8]. Fe-doped $BiVO_4$ possesses larger distortion of the local structure compared with pure $BiVO_4$, indicating that Fe doping may promote the migration of photogenerated holes and thus improve the separation of photogenerated electrons and holes in $BiVO_4$ [8].

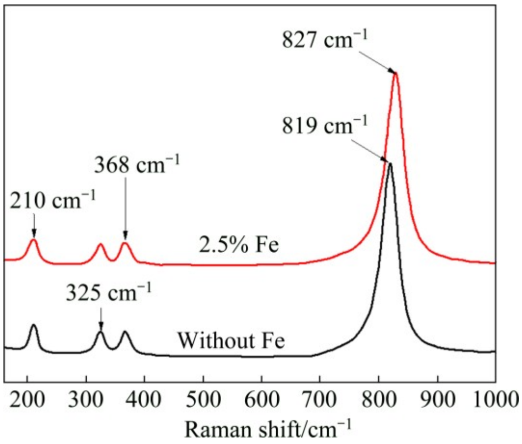

Fig. 3 Raman spectra of pure $BiVO_4$ and Fe-doped $BiVO_4$ with Fe/Bi mole ratio of 2.5%

Figures 4(a)−(c) show the SEM images of pure $BiVO_4$ and the Fe-doped $BiVO_4$ with Fe/Bi mole ratios of 2.5% and 5.0%, respectively. Obviously, all the samples possess similar 3D hierarchical flower-like structures although the Fe/Bi mole ratio varies. Moreover, these 3D hierarchical flower-like structures are actually formed by the interlacing of nanosheets with a thickness less than 50 nm. The nanosheets assemble helically and loosely to form open porous structures, which may result in large surface area and high light harvest. The BET surface areas of the pure $BiVO_4$ and the Fe-doped $BiVO_4$ with Fe/Bi mole ratios of 2.5% and 5.0% were tested to be 32.8, 33.2, 32.5 m^2/g, respectively. The open porous structures also facilitate the entry of reactants and the release of products. Moreover, the thinness of the nanosheets leads to a relatively large distortion of the unit cell due to the large surface strain, which may also promote the migration of photogenerated carriers [21]. It should be noted that the 3D hierarchical flower-like structures of Fe-doped $BiVO_4$ were obtained in the presence of SDBS. Figure 4(d) shows the SEM image of the pure $BiVO_4$ prepared in the absence of SDBS, which is composed of agglomerated particles with diameters of 300−600 nm. These results indicate that SDBS is the key factor for the formation of hierarchical flower-like structures of Fe-doped $BiVO_4$. The BET surface area of the pure $BiVO_4$ prepared in the absence of SDBS was tested to be 4.28 m^2/g.

The microstructure of Fe-doped $BiVO_4$ with a Fe/Bi mole ratio of 2.5% was further investigated by TEM and HRTEM. As shown in Fig. 5(a), the sample consists of hierarchical flower-like structures with diameters of 1.5−2 μm, which is in consistence with the SEM result. The lattice spacing of 0.46 nm in the HRTEM image (Fig. 5(b)) corresponding to the marked area in Fig. 5(a) is assigned to the interplanar spacing of (011) plane of monoclinic $BiVO_4$. It can be deduced that the lateral surfaces and the top surfaces of $BiVO_4$ nanosheets are enclosed by their (011) and (100) planes, respectively.

To explore the formation mechanism of the hierarchical flower-like structures of Fe-doped $BiVO_4$, TEM observations of the sample with a Fe/Bi mole ratio

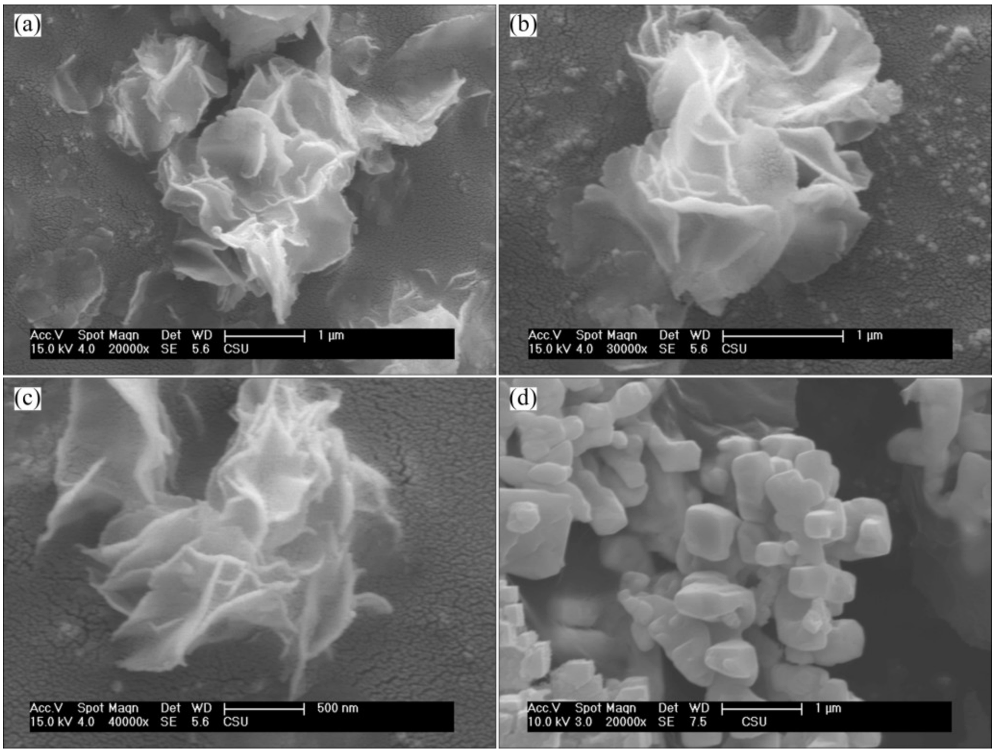

Fig. 4 SEM images of Fe-doped $BiVO_4$ with Fe/Bi mole ratios of 0 (a), 2.5% (b), and 5.0% (c) prepared in the presence of SDBS and pure $BiVO_4$ prepared in the absence of SDBS (d)

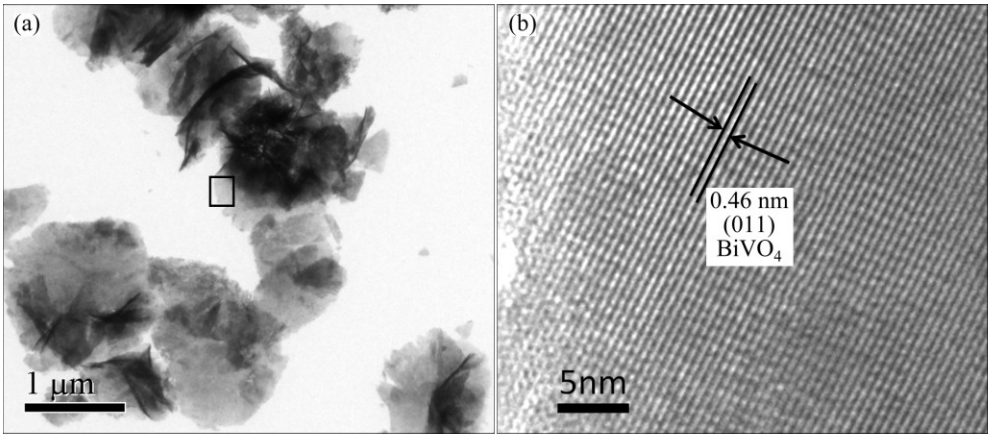

Fig. 5 TEM (a) and HRTEM (b) images of Fe-doped $BiVO_4$ with Fe/Bi mole ratio of 2.5%

of 2.5% at different hydrothermal reaction stages (2 h, 5 h and 15 h) were carried out. As shown in Fig. 6, the product obtained after 2 h of hydrothermal treatment consists of nanoplates with an average diameter of 20 nm (Fig. 6(a)). After 5 h of hydrothermal reaction, nanosheets with diameters of 400−600 nm appeared (Fig. 6(b)). As the reaction time was further prolonged to 15 h, well-defined hierarchical flower-like structures were formed (Fig. 6(c)).

On the basis of above TEM and HRTEM results, it can be concluded that the hierarchical flower-like structures of Fe-doped $BiVO_4$ are actually formed via a hierarchical assembly process. At the initial stage of hydrothermal treatment, $BiVO_4$ crystalline nuclei are formed and grow into nanoplates. Then these nanoplates further grow into 2D nanosheets, which later self assemble into hierarchical flower-like structures by oriented attachment. SDBS is a surfactant usually used to prepare nanoparticles with anisotropic shapes due to its selective adsorption on the facets of nuclei. In the present case, SDBS should have stronger interactions with (100) planes of $BiVO_4$ nuclei, resulting in the growth of 2D nanosheets. Moreover, due to strong adsorption of SDBS on the planes, the formed nanosheets do not pile up along the [100] direction due to the hindrance effects of SDBS on their top surfaces, but oriented assemble in an edge-to-edge way and curl up by a certain title angle due to the large lattice tension of nanosheets, forming flower-like structures [20,27,28].

The UV-Vis diffuse reflectance spectra of pure $BiVO_4$ and Fe-doped $BiVO_4$ with Fe/Bi mole ratio of 2.5% are presented in Fig. 7(a). Each sample shows strong absorption in the visible range in addition to the UV range. The absorption edge of pure $BiVO_4$ occurred at about 525 nm, while the absorption range of Fe-doped $BiVO_4$ is broadened to 549 nm. The bandgaps of both samples are estimated from the formula $\alpha h\nu=A(h\nu-E_g)^{n/2}$, where α, ν, E_g and A are absorption coefficient, light frequency, band gap and a constant, respectively. For $BiVO_4$, the value of n is 1 [22]. Figure 7(b) shows the plots of $(\alpha h\nu)^2$ versus photon energy ($h\nu$), from which we can estimate the energy of the bandgap of the samples. The estimated E_g of pure $BiVO_4$ and Fe-doped $BiVO_4$ with a Fe/Bi mole ratio of 2.5% are 2.36 eV and 2.26 eV, respectively. The bandgap energy decreases with doping Fe ions in $BiVO_4$, indicating that Fe-doping may enhance the absorption of $BiVO_4$ in the visible light zone and improve the visible light photocatalytic activity of $BiVO_4$.

The photodegradation efficiencies of MB as a function of irradiation time by the samples prepared in the presence and absence of SDBS, as well as without photocatalyst, are presented in Fig. 8. It can be seen that all the samples show visible-light-responsive photocatalytic activities, since the concentrations of MB reduce faster in the presence of those samples than photolysis. It should be noted that the samples prepared in the presence of SDBS show higher photocatalytic activities than that prepared in the absence of SDBS. Generally, the overall photocatalytic activity of a semiconductor is primarily decided by surface area, photoabsorption ability, and the separation and transporting rate of photogenerated electrons and holes in the catalysts [29]. The higher photocatalytic activities of the sample prepared in the presence of SDBS compared with that prepared in the absence SDBS may be attributed to its unique morphology. The hierarchical flower-like structure composed of nanosheets results in larger surface areas and higher light harvest [22]. Moreover, the thinness and the distortion of the unit cell for the nanosheets facilitate the migration of photogenerated electrons and holes from inside to the

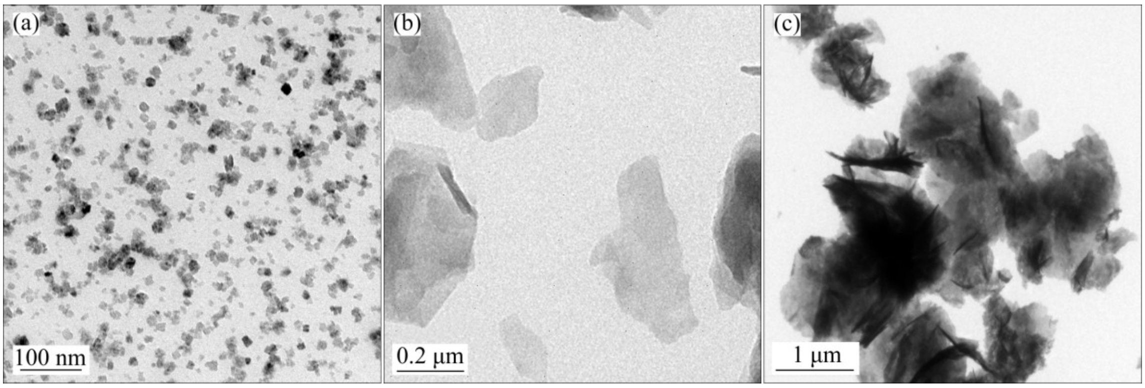

Fig. 6 TEM images of Fe-doped $BiVO_4$ with Fe/Bi mole ratio of 2.5% obtained at different hydrothermal reaction stages: (a) 2 h; (b) 5 h; (c) 15 h

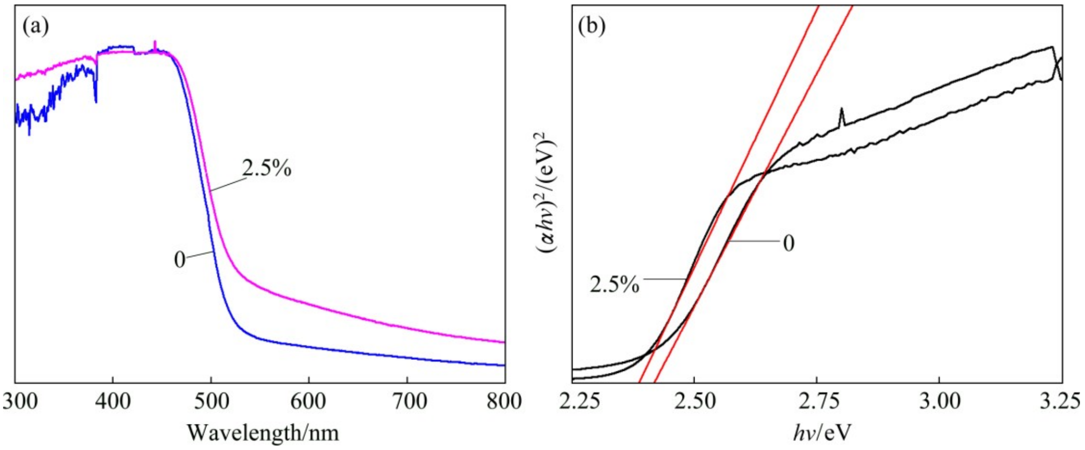

Fig. 7 UV-Vis diffuse reflectance spectra of pure $BiVO_4$ and Fe-doped $BiVO_4$ with Fe/Bi mole ratio of 2.5% (a) and plots of $(\alpha h\nu)^2$ vs photon energy ($h\nu$) (b)

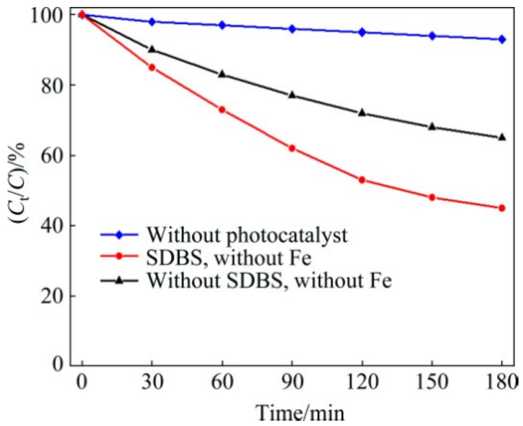

Fig. 8 Photocatalytic efficiencies of $BiVO_4$ samples prepared in the presence and absence of SDBS

surface, retarding the recombination of photogenerated electrons and holes [21]. All these may improve the quantum yield and the photocatalytic activity of hierarchical flower-like $BiVO_4$.

Figure 9 shows the photocatalytic efficiencies of the hierarchical flower-like Fe-doped $BiVO_4$ with different Fe/Bi mole ratios. The sample with a Fe/Bi mole ratio of 2.5% shows the highest photocatalytic efficiency, indicating that the photocatalytic activity first increases with increasing the Fe doping content then reaches an optimum level. Further increasing the amount of Fe beyond this level slows down MB photodegradation. The enhanced photocatalytic acvitities of the Fe-doped $BiVO_4$ samples may be attributed to the following reasons. Firstly, Fe doping reduces the bandgap energy of $BiVO_4$. The visible light response range of $BiVO_4$ is widened, and the utilization of visible light is improved. Secondly, the substitution of V^{5+} by Fe^{3+} results in lattice distortion and enlarges the distortion of the local structure due to the different ionic radii of V^{5+} and Fe^{3+}, which improve the migration and separation of photogenerated carriers, leading to a higher quantum yield. Thirdly, XPS results reveal that Fe doping creates many oxygen vacancies, which act as electron trappers to retard the recombination of photogenerated electrons and holes, further improving the quantum efficiency of $BiVO_4$ [11]. The harmful effect of excess doping content of Fe may be attributed to the fact that further increasing the amount of Fe beyond optimum level may result in the enrichment of iron. The enriched iron may act as recombination centers for electrons and holes, decreasing the quantum yield of $BiVO_4$ [12].

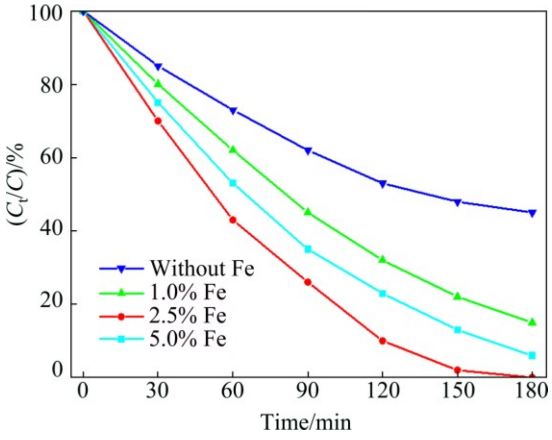

Fig. 9 Photocatalytic efficiencies of flower-like Fe-doped $BiVO_4$ samples with different Fe/Bi ratios

4 Conclusions

1) Fe-doped $BiVO_4$ with hierarchical flower-like structures was prepared by a SDBS assisted hydrothermal method.

2) SEM, TEM and HRTEM results showed that the hierarchical flower-like structures of Fe-doped $BiVO_4$ were actually formed by the interlacing of nanosheets with a thickness less than 50 nm. The time-dependent experiments indicated that the selective adsorption of SDBS on the (100) facet of m-$BiVO_4$ played a key role in the formation and oriented assembly of nansheets.

3) Flower-like Fe doping $BiVO_4$ showed much higher visible-light-driven photocatalytic efficiency for degradation of MB compared with pure $BiVO_4$. And the sample with Fe/Bi mole ratio of 2.5% showed the highest photocatalytic efficiency.

4) Fe doping creates oxygen vacancies and enlarges the distortion of the local structure of $BiVO_4$, improving the quantum yield of $BiVO_4$. The large surface area and porous structure were also responsible for the enhanced photocatalytic activity of Fe-doped flower-like $BiVO_4$.

References

[1] HUANG Xiao-jun, YAN Xin, WU Hai-yan, FANG Ying, MIN Ya-hong, LI Wen-sheng, WANG Shuang-yin, WU Zhen-jun. Preparation of Zr-doped $CaTiO_3$ with enhanced charge separation efficiency and photocatalytic activity [J]. Transactions of Nonferrous Metals Society of China, 2016, 26(2): 464−471.

[2] DU Jun, GU Xin, WU Qi, LIU Jiao, GUO Hai-zhi, ZOU Jian-guo. Hydrophilic and photocatalytic activities of Nd-doped titanium dioxide thin films [J]. Transactions of Nonferrous Metals Society of China, 2015, 25(8): 2601−2607.

[3] XU Jing-jing, CHEN Min-dong, FU De-gang. Preparation of bismuth oxide/titania composite particles and their photocatalytic activity to degradation of 4-chlorophenol [J]. Transactions of Nonferrous Metals Society of China, 2011, 21(2): 340−345.

[4] REN Jia, WAN Wen-zhong, SU Song-mei. Enhanced photocatalytic activity of Bi_2WO_6 loaded with Ag nanoparticles under visible light irradiation [J]. Applied Catalysis B: Environmental, 2009, 92(1): 50−55.

[5] MADHUSUDAN P, ZHANG J, CHENG B, LIU G. Photocatalytic degradation of organic dyes with hierarchical $Bi_2O_2CO_3$ microstructures under visible-light [J]. Cryst Eng Comm, 2013, 15(2): 231−240.

[6] GUAN Mei-li, MA De-kun, HU Sheng-wei, CHEN Yan-jun, HUANG Shao-ming. From hollow olive-shaped $BiVO_4$ to n-p

core-shell $BiVO_4@Bi_2O_3$ microspheres: Controlled synthesis and enhanced visible-light-responsive photocatalytic properties [J]. Inorganic Chemistry, 2010, 50(3): 800−805.

[7] SHANG Meng, WANG Wen-zhong, REN Jia, ZHANG Ling, CHANG Jiang. A novel $BiVO_4$ hierarchical nanostructure: Controllable synthesis, growth mechanism, and application in Photocatalysis [J]. Crystengcomm, 2010, 12(12): 1754−1758.

[8] YU Jian-qiang, KUDO A. Effects of structural variation on the photocatalytic performance of hydrothermally synthesized $BiVO_4$ [J]. Advanced Functional Materials, 2006, 16(16): 2163−2169.

[9] MADHUSUDAN P, RAN J, ZHANG J, YU J, LIU G. Novel urea assisted hydrothermal synthesis of hierarchical $BiVO_4/Bi_2O_2CO_3$ nanocomposites with enhanced visible-light photocatalytic activity [J]. Applied Catalysis B: Environmental, 2011, 110: 286−295.

[10] LI Yan-qing, JING Tao, LIU Yuan-yuan, HUANG Bai-biao, DAI Ying, ZHANG Xiao-yang, QIN Xiao-yan, WHANGBO M H. Enhancing the efficiency of water oxidation by boron-doped $BiVO_4$ under visible light: Hole trapping by BO_4 tetrahedra [J]. Chem Plus Chem, 2015, 80(7): 1113−1118.

[11] WANG Min, CHE Yin-sheng, NIU Chao, DANG Ming-yan, DONG Duo. Lanthanum and boron co-doped $BiVO_4$ with enhanced visible light photocatalytic activity for degradation of methyl orange [J]. Journal of Rare Earths, 2013, 31(9): 878−884.

[12] WANG C Y, BÖTTCHER C, BAHNEMANN D W, DOHRMANN J K. A comparative study of nanometer sized Fe(III)-doped TiO_2 photocatalysts: Synthesis, characterization and activity [J]. Journal of Materials Chemistry, 2003, 13(9): 2322−2329.

[13] YEOM T H, CHOH S H, DU M L, JANG M S. EPR study of Fe^{3+} impurities in crystalline $BiVO_4$ [J]. Physical Review B, 1996, 53(6): 3415−3421.

[14] FAN H, WANG D, WANG L, LI H, WANG P, JIANG T, XIE T. Hydrothermal synthesis and photoelectric properties of $BiVO_4$ with different morphologies: An efficient visible-light photocatalyst [J]. Applied Surface Science, 2011, 257(17): 7758−7762.

[15] HOJAMBERDIEV M, ZHU G, KADIROVA ZC, HAN J, LIANG J, ZHOU J, WEI X, LIU P. Morphology-controlled growth of $BiVO_4$ crystals by hydrothermal method assisted with ethylene glycol and ethylenediamine and their photocatalytic activity [J]. Materials Chemistry and Physics, 2015, 165: 188−195.

[16] GUO Y, YANG X, MA F, LI K, XU L, YUAN X, GUO Y. Additive-free controllable fabrication of bismuth vanadates and their photocatalytic activity toward dye degradation [J]. Applied Surface Science, 2010, 256(7): 2215−2222.

[17] ZHOU L, WANG W, ZHANG L, XU H, ZHU W. Single-crystalline $BiVO_4$ microtubes with square cross-sections: Microstructure, growth mechanism, and photocatalytic property [J]. The Journal of Physical Chemistry C, 2007, 111(37): 13659−13664.

[18] MADHUSUDAN P, KUMAR MV, ISHIGAKI T, TODA K, UEMATSU K, SATO M. Hydrothermal synthesis of meso/macroporous $BiVO_4$ hierarchical particles and their photocatalytic degradation properties under visible light irradiation [J]. Environmental Science and Pollution Research, 2013, 20(9): 6638−6645.

[19] LU Y, SHANG H, SHI F, CHAO C, ZHANG X, ZHANG B. Preparation and efficient visible light-induced photocatalytic activity of m-$BiVO_4$ with different morphologies [J]. Journal of Physics and Chemistry of Solids, 2015, 85: 44−50.

[20] LI Yuan-yuan, LIU Jin-ping, HUANG Xin-tang, LI G. Hydrothermal synthesis of Bi_2WO_6 uniform hierarchical microspheres [J]. Crystal Growth & Design, 2007, 7(7):1350−1355.

[21] LI Zhang, CHEN Dai-rong, JIAO Xiu-ling. Monoclinic structured $BiVO_4$ nanosheets: Hydrothermal preparation, formation mechanism, and coloristic and photocatalytic properties [J]. The Journal of Physical Chemistry B, 2006, 110 (6): 2668−2673.

[22] LI Hai-bin, LIU Guo-cong, DUAN Xue-chen. Monoclinic $BiVO_4$ with regular morphologies: Hydrothermal synthesis, characterization and photocatalytic properties [J]. Materials Chemistry and Physics, 2009, 115(1): 9−13.

[23] ZHOU Y, VUILLE K, HEEL A, PROBST B, KONTIC R, PATZKE G R. An inorganic hydrothermal route to photocatalytically active bismuth vanadate [J]. Applied Catalysis A: General, 2010, 375(1): 140−148.

[24] DUAN Yu-lu, ZHOU Li-qi, XU Guo-fu, ZHANG Hui-ying, LI Xu, LIU Xiao-he. Preparation and characterization of ZnSe/CdSe core-shell microspheres [J]. Transactions of Nonferrous Metals Society of China, 2015, 25(5): 1559−1567.

[25] KUDO A, KEIKO O, HIDEKI K. A novel aqueous process for preparation of crystal form-controlled and highly crystalline $BiVO_4$ powder from layered vanadates at room temperature and its photocatalytic and photophysical properties [J]. Journal of the American Chemical Society, 1999, 121 (49): 11459−11467.

[26] YU Jian-qiang, ZHANG Yan, KUDO A. Synthesis and photocatalytic performances of $BiVO_4$ by ammonia co-precipitation process [J]. Journal of Solid State Chemistry, 2009, 182 (2): 223−228.

[27] ZHOU Yong, TIAN Zhong-ping, ZHAO Zong-yan, LIU Qi, KOU Jia-hui, CHEN Xiao-yu, GAO Jun, YAN Shi-cheng, ZOU Zhi-gang. High-yield synthesis of ultrathin and uniform Bi_2WO_6 square nanoplates benefitting from photocatalytic reduction of CO_2 into renewable hydrocarbon fuel under visible light [J]. ACS Applied Materials & Interfaces, 2011, 3(9): 3594−3601.

[28] LI Yuan-yuan, LIU Jin-ping, HUANG Xin-tang. Synthesis and visible-light photocatalytic property of Bi_2WO_6 hierarchical octahedron-like structures [J]. Nanoscale Research Letters, 2008, 3(10): 365−371.

[29] HE Zhi-qiao, SHI Yuan-qiao, GAO Chao, WEN Lina, CHEN Jian-meng, SONG Shuang. BiOCl/$BiVO_4$ p–n heterojunction with enhanced photocatalytic activity under visible-light irradiation [J]. The Journal of Physical Chemistry C, 2013, 118(1): 389−398.

多层级花状铁掺杂 $BiVO_4$ 的水热法制备与光催化性能

李海斌，张 健，黄国游，付圣豪，马 超，王白羽，黄倩如，廖红卫

长沙理工大学 材料科学与工程学院，长沙 410114

摘 要：以 $Bi(NO_3)_3$、Na_3VO_4 和 $Fe(NO_3)_3$ 为原料，以十二烷基苯环酸钠为结构导向剂，采用水热法制备了铁掺杂 $BiVO_4$。利用 XRD、SEM、TEM、HRTEM 以及紫外−可见漫反射光谱(UV-Vis)对样品进行结构、形貌及光吸收性能分析。结果表明：铁掺杂 $BiVO_4$ 具有由纳米片组装而成的多层级花状结构。SDBS 在 $BiVO_4$(100)晶面的选择性吸附是花状结构形成的关键原因。适量铁离子进入 $BiVO_4$ 晶格后，导致 $BiVO_4$ 发生晶格畸变，加大了 $BiVO_4$ 局域结构的变形，形成了氧空位，并缩小了 $BiVO_4$ 的带隙，从而促进 $BiVO_4$ 光生电子和空穴的分离，拓宽 $BiVO_4$ 的可见光吸收范围，有效提高 $BiVO_4$ 的光催化活性。当铁掺杂浓度为 2.5%时，样品对甲基蓝的光催化活性最高。

关键词：$BiVO_4$；水热法；铁掺杂；光催化

(Edited by Yun-bin HE)